Development of fast dissolving polymer-based microneedles for delivery of an antigenic melanoma cell membrane

Lobita, Maria C.; El-Sayed, Nesma; Pinto, João F.; Santos, Hélder A.

Published in:
International Journal of Pharmaceutics

DOI:
10.1016/j.ijpharm.2023.123143

Publication date:
2023

International Journal of Pharmaceutics 642 (2023) 123143

Contents lists available at ScienceDirect

International Journal of Pharmaceutics

journal homepage: www.elsevier.com/locate/ijpharm

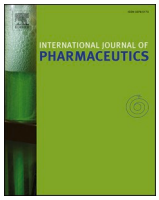

Development of fast dissolving polymer-based microneedles for delivery of an antigenic melanoma cell membrane

Maria C. Lobita [a,b], Nesma El-Sayed [c,d,*], João F. Pinto [e], Hélder A. Santos [a,b,c,*]

[a] Department of Biomedical Engineering, University Medical Center Groningen, University of Groningen, 9713 AV Groningen, The Netherlands
[b] W.J. Kolff Institute for Biomedical Engineering and Materials Science, University Medical Center Groningen, University of Groningen, 9713 AV Groningen, The Netherlands
[c] Drug Research Program, Division of Pharmaceutical Chemistry and Technology, Faculty of Pharmacy, P.O. Box 56 (Viikinkaari 5 E), University of Helsinki, FI-00014 Helsinki, Finland
[d] Department of Pharmaceutics, Faculty of Pharmacy, Alexandria University, 21521 Alexandria, Egypt
[e] iMED-Research Institute for Medicines, Faculty of Pharmacy, University of Lisbon, Av. Prof. Gama Pinto, 1640-003 Lisbon, Portugal

ARTICLE INFO

Keywords:
Dissolving microneedles
Immunotherapy
Micromolding
Microneedles
Transdermal delivery

ABSTRACT

Delivery of cancer cell membranes (CM) is a new approach for the activation of the immune system and the induction of immunotherapy of cancer. Local delivery of melanoma CM into skin can induce efficient immune stimulation of antigen presenting cells (APCs), such as dendritic cells. In the current study, fast dissolving microneedles (MNs) were developed for the delivery of melanoma B16F10 CM. Two polymers were tested for the fabrication of MNs: poly(methyl vinyl ether-co-maleic acid) (PMVE-MA) and hyaluronic acid (HA). The incorporation of CM in MNs was achieved through coating of the MNs using a multi-step layering procedure or the micromolding technique. The CM loading and its stabilization were improved by adding sugars (sucrose and trehalose) and a surfactant (Poloxamer 188), respectively. In an *ex vivo* experiment, both PMVE-MA and HA showed fast dissolutions (<30 s) after insertion into porcine skin. However, HA-MN showed better mechanical properties, namely improved resistance to fracture when submitted to a compression force. Overall, a B16F10 melanoma CM-dissolving MN system was efficiently developed as a promising device suggesting further studies in immunotherapy and melanoma applications.

1. Introduction

Transdermal drug delivery is an attractive route of administration, considering drugs do not go through enzymatic degradation. Moreover, transdermal delivery is appealing to the patients due to the painless delivery of a variety of cargos (Prausnitz, 2004). However, the stratum corneum (SC)'s characteristics, such as lipophilic structure with low permeability, hinders the delivery of hydrophilic drugs, peptides, and macromolecules (Aich et al., 2022).

Microneedles (MNs) represent a micron-sized array of needles with a length up to 1500 μm, attached to a flat support, capable of penetrating, with minimal invasion of the outer layer of the skin, i.e., the SC (Amani et al., 2021; D'Amico et al., 2023). It allows the delivery of a high diversity compounds throughout the formation of microscopic pores in the skin (Zhang et al., 2020). Polymers have been widely used due to their diverse physicochemical and mechanical properties (Sabbagh and Kim, 2022; Zhu et al., 2022). Ideally, polymeric MNs should be biocompatible and non-immunogenic, hard enough to pierce the SC, controlling the release of cargos, requiring mild conditions when fabricated to protect sensitive biologicals, such as proteins and peptides with therapeutic value (Gera and Burra, 2022; Sadeqi et al., 2022). Three groups of polymers are primarily used to fabricate polymeric MNs: swellable, biodegradable and dissolving polymers (Singh et al., 2019).

Dissolving microneedles (DMNs) are distinctive systems consisting of a fast-dissolving polymer after contact with skin fluids, allowing the delivery of therapeutic agents (Bauleth-Ramos et al., 2023; Leone et al., 2019). It is essential to consider the properties of the dissolvable polymers to manufacture MNs with efficient drug delivery, optimized mechanical strength to pierce the SC, preservation of the bioactivity, and stability of biological cargos (Ali et al., 2022). Examples of such

* Corresponding authors at: Drug Research Program, Division of Pharmaceutical Chemistry and Technology, Faculty of Pharmacy, P.O. Box 56 (Viikinkaari 5 E), University of Helsinki, FI-00014 Helsinki, Finland (N. El-Sayed). Department of Biomedical Engineering, University Medical Center Groningen, University of Groningen, 9713 AV Groningen, The Netherlands (H.A. Santos).
E-mail addresses: nesma.ibrahim@helsinki.fi (N. El-Sayed), h.a.santos@umcg.nl (H.A. Santos).

https://doi.org/10.1016/j.ijpharm.2023.123143
Received 3 April 2023; Received in revised form 9 June 2023; Accepted 11 June 2023
Available online 15 June 2023

polymers include dextran, hydroxypropylmethylcellulose (HPMC), carboxymethylcellulose (CMC), hyaluronic acid (HA), and poly(methylvinylether/maleic anhydride) (PMVE-MA, Gantrez®). PMVE-MA is a synthetic copolymer of methylvinyl and maleic anhydride (Huang et al., 2020; Mbituyimana et al., 2022). It is suitable for different pharmaceutical applications, as it can be used as film former, emulsion stabilizer, thickening agent, dispersing agent, and denture adhesive (Demir et al., 2017). HA is a water-soluble linear anionic polysaccharide, comprised of two alternating saccharide units of glucuronic acid linked to N-acetylglucosamine (Cheng et al., 2022). Hyaluronic acid is known for its biodegradability, biocompatibility, and high viscoelasticity (Wang et al., 2022). It is a non-toxic and non-inflammatory polysaccharide (Kim et al., 2022). It exists in three molecular weights: high molecular weight (HMW ~ 10^7 Da), the most considered for skin applications (Schmidt et al., 2021), medium molecular weight (MMW ~ 20000 Da), and low molecular weight (LMW ~ 800–3200 Da). The molecular weight of the polymer has different impact on the immune system. For instance, the HA-LMW can stimulate the IS, activating immune cells, such as macrophages and DCs, and thus, it can be used as a potential component for immunotherapy (Baeva et al., 2014).

There are several fabrication methods to produce polymeric MNs (Liu et al., 2020). Micromolding is the most common method for manufacturing MNs due to its reproducibility, ease of scaling up, and low cost (Guillot et al., 2020; Tran et al., 2021). This method can be summarized in the following steps: (1) preparing a MN template to assemble the negative molds from a positive master mold; (2) casting polymers into the molds by centrifugation; (3) elimination of bubbles using vacuuming or ultrasounds; (4) solidification by drying or photocrosslinking; and (5) removing the MNs from the molds (Ita, 2017; Park et al., 2005). There are three main parameters to be considered to manufacture MNs with the appropriate mechanical properties: polymer MW, concentration in solutions for preparation, and balance between viscoelasticity and brittleness of the MN (Hong et al., 2013; Park et al., 2007).

The materials used for DMNs fabrication are widely available, cost-effective, and do not need special conditions of processing, such as high temperatures (Sabri et al., 2020). In addition, DMNs do not leave behind biohazardous sharp tips, because they completely dissolve after penetration into the skin. Furthermore, DMNs have higher capacity for drug loading, when compared with other types of MNs (Dalvi et al., 2021).

The skin is responsible for critical functions in the body. It is divided into three main layers: the SC, the epidermis, and the dermis (Rawlings and Harding, 2004). The SC, made of dead keratinized cells, with a thickness between 10 and 20 μm, is selectively permeable. Beneath the SC is the epidermis, comprising keratinocytes, melanocytes and rich in immune cells, such as primary APCs, specific dendritic cells (DCs), and Langerhans cells (El-Sayed et al., 2020). The dermis with a thickness between 3 and 5 mm contains immune cells, in a lower density when compared with the epidermis, nerve terminations, blood vessels, lymphatic vessels, and sweat and hair glands (Guillot et al., 2023).

Melanoma is one of the most aggressive forms of skin cancer (Imlimthan et al., 2021).Its incidence continues to rise worldwide, accounting for more than 70 % of skin cancer(Liu et al., 2022). Traditional treatments include surgical removal, chemotherapy, radiotherapy, photodynamic therapy, and the use of tyrosine kinase inhibitors interfering with the intracellular signalling pathways limiting the tumoral expansion (Davis et al., 2019). However, these approaches fail in the presence of metastasis and in later-stage melanoma, requiring new approaches (Naing and Hajjar, 2018), namely immunotherapy, which has proved useful to overcome the limitations of the traditional treatments (Fusciello et al., 2019). It is a biological based therapy where the immune system (IS) is stimulated to fight against cellular diseases (Lesterhuis et al., 2011).

DMNs have been widely applied in immunotherapy, particularly in antigens delivery to DCs, presenting them to T cells to stimulate the immune system response (Yenkoidiok-Douti et al., 2021) (Matsuo et al., 2012). For example, Park *et al.* developed DMNs loaded with nanoparticles coated with the cancer cell membrane (CM), using the CM as an antigen to activate the immune system, through APCs, to fight cancer (Park et al., 2021). Zeng *et al.* developed a polyelectrolyte multilayer as a platform for the cancer vaccine components on MN patches for intradermal delivery (Zeng et al., 2017). However, these new systems needed to be combined with other therapies to become effective. To overcome these limitations, the immune system should be potentiated enough to destroy the cancer cells.

In order to understand the positive impact of creating an innovative transdermal delivery system to stimulate immunotherapy against melanoma, the present study focuses on the development and optimization of DMNs loaded with a cancer CM derived from a melanoma cell line, B16F10. The hypothesis relies on the possibility to deliver CM into the epidermis, which is rich in immune cells, using DMNs, with the ultimate purpose of promoting the immune system activation, through DCs, against cancer. In this study, to support the hypothesis, DMNs were fabricated by micromolding, once several formulation and processing parameters were considered, in combination with extracts of isolated CM from cancer cells, used to coat the DMNs.

2. Materials and methods

2.1. Materials

Hyaluronic acid (HA MW 20 kDa, Creative PEGWorks, China), poly (methyl vinyl ether-alt-maleic acid) (PMVE-MA, Sigma, Germany), poloxamer 188 (Kolliphor P 188 micro, BASF, Germany), trehalose dihydrate (Sigma, USA), carboxymethylcellulose sodium salt (CMC, Sigma, USA), sucrose (Sigma, Switzerland), ammonium acetate (LiChropur, Supelco, Germany), melanoma cell line B16F10 (ATCC, US), growth cell medium solution mixture of Dulbecco's Modified Eagle's Medium (DMEM, Cytiva, USA) and fetal bovine serum (FBS, Cytiva, USA), ethylenediaminetetraacetic acid (EDTA; Life Technologies, USA), phosphate buffered saline (PBS, Cytiva, USA).

2.2. Methods

2.2.1. Dissolving MN fabrication

The MNs were prepared by a micromolding procedure. Briefly, 20 μL of the aqueous solution of 20 % (w/v) PMVE-MA, was pipetted on the top of the negative mold (MNs: 800 μm (height) and 200 μm (Base) and pitch: 500 μm; MICROPOINT, Singapore), followed by centrifugation for 10 min at 2000 rcf (relative centrifugal force) using a swing bucket centrifuge (centrifuge 5415D, Eppendorf, Germany) (Leone et al., 2019; Park et al., 2005). Afterwards, another 20 μL of PMVE-MA solution were placed on the top of the mold prior to centrifugation at 180 rcf. To form the base layer of MNs, an additional 130 μL of the 20 % polymer solution was laid on the top of the molds followed by drying in a desiccator at

Table 1
MNs prepared using 20 % PMVE-MA using the common protocol.

	Drying Process	Centrifugation speed (rcf)	Fabrication method
MNg	Desiccator for two days	2,000	Common protocol
MN1	Desiccator for two days	1,000	
MN2	Desiccator for two days	500	
MN3	Vacuum during 4.5 h Desiccator overnight	2,000	
MN4	–	2,000	MNs and patches produced separately

room temperature for 2 days (El-Sayed et al., 2020).

Modifications to the fabrication process are described in Table 1. To evaluate the influence of centrifugation speed on the formation of MNs, two different speeds were tested using the general protocol: 1,000 rcf (MN1) and 500 rcf (MN2). Furthermore, the drying process was altered in MN3 (for the first 4.5 h, the MNs were placed in the vacuum oven, followed by completing the drying process in the desiccator, at room temperature. In MN4, the patch, i.e., the baking layer, and the MNs were fabricated individually. The patch base was formed by adding 150 μL of PMVE-MA solution into the mold followed by drying in the desiccator for 2 days. The MNs were prepared according to the standard procedure using another separate mold. The base layer was detached from the mold and moved to the top of the other mold containing the MNs that were not solidified yet. With the force of a fingertip, compression was applied to bind the MNs and the base together. After the drying process, in the desiccator for 2 days, all MNs were removed from the molds and observed in a light microscope (EVOS™ XL, Thermo Fisher Scientific, USA).

2.2.2. Extraction of the cell membrane from cancer cells

B16F10 melanoma cell line was cultured in 12 mL of DMEM containing 10 % of FBS at 5 % of CO_2 and 37 °C. The cells were harvested after observation under the microscope and the confluence confirmed (80 %). 10 mL of cold PBS – EDTA was added to the flasks and placed in the incubator for 5–10 min, 5 % CO_2, 37 °C, followed by collection of cells into Falcon® tubes. In order to collect the cell pellet, the Falcon® tubes were placed in the centrifuge for 5 min at 250 rcf. The pellet was resuspended in 10 mL of PBS, the supernatant was discarded, and 400 μL of the suspension was collected for cell counting. The cell suspension was centrifuged, a volume equivalent to a final concentration of 3×10^6 cells/mL was considered, and the pellet was resuspended in lysis buffer. Homogenization was accomplished by placing the samples in a bath sonicator (Transsonic T700, Germany) for 2 min, followed by centrifugation in 1 mL Eppendorf tubes for 5 min at 3,200 rcf. The supernatant was saved in ultracentrifuge tubes, and the pellet was resuspended in 1 mL of lysis buffer, with the sonication step and centrifugation process repeated for 6 min at 3,200 rcf, to maximize the collection of CM. The supernatant was collected in the same ultracentrifuge tubes. Ultracentrifugation was performed (Optima L-80 XP, Beckman Coulter, USA) for 30 min, 4 °C, at 21,000 rcf. New ultracentrifuge tubes were used to collect the supernatant and moved to the ultracentrifuge to start the process for 15 min at 45,000 rcf, 4 °C. Then, the CM was obtained in the pellet and was further redispersed in suitable dispersant for loading the MNs.

2.2.3. MN loading with CM

2.2.3.1. Coating technique. In this three-step procedure (Fig. 1**A**), the CM was labelled with CellMask™ orange and dispersed in a stabilizing solution (5 % trehalose, 5 % sucrose, 0.5 % poloxamer 188 (P188)) to give rise to a concentration of CM extracted from 7.6×10^6 cells/mL. Firstly, 20 μL of the solution was added to the top of the negative mold, followed by centrifugation for 10 min at 500 rcf. The molds were placed in the vacuum oven for 30 min at 400 mbar. This first step was repeated

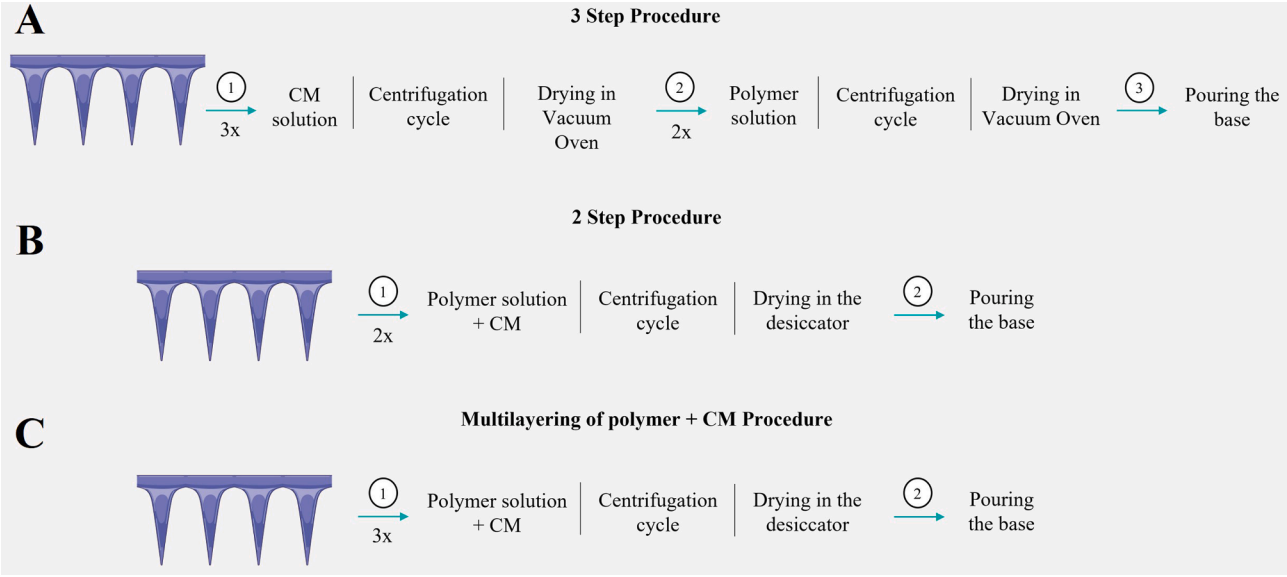

Fig. 1. Schematic illustration of CM-MNs fabrication using the coating technique (A), the encapsulation technique (B) and the multilayering protocol for the CM-loaded MNs preparation (C).

Table 2
Modifications applied to the CM-coated MNs formulation.

	Stabilizing Solution				Polymer		CM	Molds
	Water (μL)	Sucrose (%)	Trehalose (%)	P188 (%)	PMVE-MA (%)	HA (%)	[CM]	Pre-treatment O_2
MNg1	–	5	5	0.5	20	–	1CM	–
MN5	200	–	–	–	20	–	1CM	–
MN6	–	5	5	–	20	–	1CM	–
MN7	–	5	5	0.5	–	20	1CM	–
MN8	–	5	5	0.5	–	20	1CM	Plasma surface treatment
MN9	–	10	10	1	–	20	1CM	–
MN10	–	10	10	1	–	20	3CM	–

* 1 CM is equivalent to the cell membrane extracted from 7.6×10^6 cells/mL.

two more times to increase the amount of CM present in the walls of the MN mold. Secondly, 20 μL of PMVE-MA 20 % (w/v) was poured into the molds and placed in the centrifuge for 10 min at 1,000 rcf to be stored under vacuum at 400 mbar for 30 min. The second step was repeated one more time. In the final step, 30 μL of the polymer solution was laid on top of the molds and the molds were centrifuged for 10 min at 180 rcf. The base layer was formed by adding 130 μL of PMVE-MA 20 % on the top of the molds followed by drying in desiccator for 3 days at room temperature. The MNs were removed from the molds and visualized under a confocal laser scanning microscope (CLSM, SP8 upright, Leica, Germany) using HC PL APO 10x/0.4 CS2 objective lens, an excitation laser of 552 nm and an emission filter of 560–700 nm. All examinations were carried out at room temperature.

In Table 2 are denoted all the variations applied to the protocol for coated MNs. PMVE-MA 20 % was the selected polymer to fabricate the MNg1, MN5, and MN6. For MN7, MN8, MN9, and MN10, the chosen polymer for MNs production was HA 20 %. As described in Table 2, the MNg1 represents the general protocol. The CM was dispersed in water as a control (MN5), the CM solution was combined with sucrose and trehalose (MN6), a surfactant, P188, was added to the sugar solution containing CM (MN7). The same stabilizing solution used in MN7 was selected to fabricate HA MNs (MN8), using HA 20 %. In order to increase MN8 hydrophilicity, a pre-treatment with O_2 plasma was applied to the molds. To improve the uniformity of CM distribution, the concentrations of the additives (sugar and surfactant) were duplicated in MN9 and MN10, respectively. In MN10, to evaluate the possibility of loading a higher amount of CM, the concentration of CM was triplicated.

2.2.3.2. Encapsulation technique. The MNs were produced by a two-step procedure (Fig. 1**B**). The CM was dispersed in a stabilizing/polymeric solution made of sucrose (2.5 %), trehalose (2.5 %), P188 (0.25 %), and PMVE-MA (15 %). Initially, 20 μL of cell membrane suspension labeled with a CellMask^{TM} orange was added to the top of the molds and centrifuged twice at 1,000 rcf for 10 min. Subsequently, the MNs were dried in a desiccator, at room temperature, overnight. The base layer was formed by adding 130 μL of PMVE-MA (20 %, w/v) to the top of each mold, followed by drying in a desiccator for 5 days. Afterwards, all the MNs were peeled off the molds and observed under the confocal microscope, as before.

Modifications were applied to the procedure, as indicated in Table 3. MNg2 symbolizes the general loading protocol as explained. In MN12, the polymer, sugars and surfactant concentrations were duplicated. HA was the selected polymer in MN13 and MN14. For MN14 the protocol was changed to a multilayering procedure of the CM/polymer mixture (Fig. 1**C**).

2.2.4. Mechanical properties

In order to compare the mechanical properties of PMVE-MA, and HA MNs, the following studies were performed.

2.2.4.1. Load at break. Both PMVE-MA MN, and HA MNs were prepared using 20 % (w/v) polymer solution. The patches were fixed in the probe of the Texture Analyser (CT3, Brookfield, USA) by a double-sided tape, and compression was applied against the metal surface for 30 s at a speed of 0.5 mm/s, for a maximum force of 20 N, which is the average force for pressing the thumb, according to Larrañeta *et al.* (Larrañeta et al., 2014). All the MNs were observed under the microscope before and after the force application (Fig. 2**A**).

Table 3
Modifications in the protocol of CM-MNs using the encapsulation technique.

	Stabilizing Solution					Base Polymer		CM	Procedure Steps
	Sucrose (%)	Trehalose (%)	P188 (%)	PMVE-MA (%)	HA (%)	PMVE-MA (%)	HA (%)	[CM]	Multilayering of polymer + CM procedure
MNg2	2.5	2.5	0.25	15	–	20	–	1CM	–
MN12	5	5	0.5	30	–	20	–	1CM	–
MN13	5	5	0.5	–	20	–	20	1CM	–
MN14	5	5	0.5	–	20	–	20	1CM	Adjustment of steps

* 1 CM is equivalent to cell membrane extracted from 7.6 × 10^6 cells/mL.

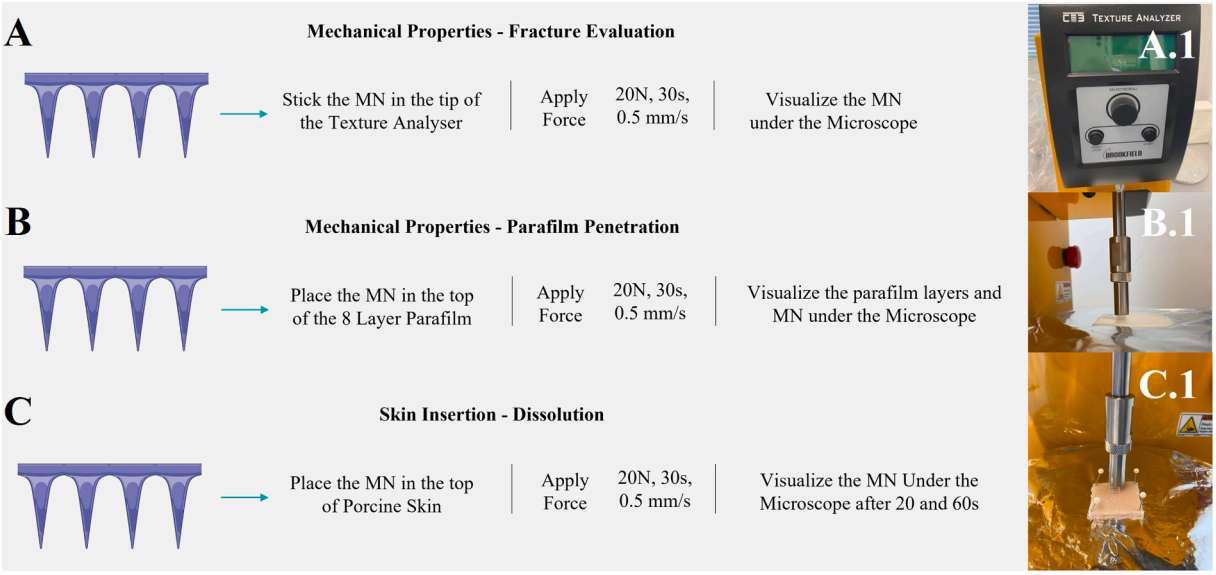

Fig. 2. Illustration presenting the relevant steps in the study of MNs properties. (A) Fracture evaluation; (A.1) Texture Analyser as the selected equipment; (B) Parafilm penetration; (B.1) Insertion in the 8-layer Parafilm by the MN patch using Texture Analyser; (C) MNs dissolution after skin insertion; (C.1) MN patch insertion in porcine skin using Texture Analyser.

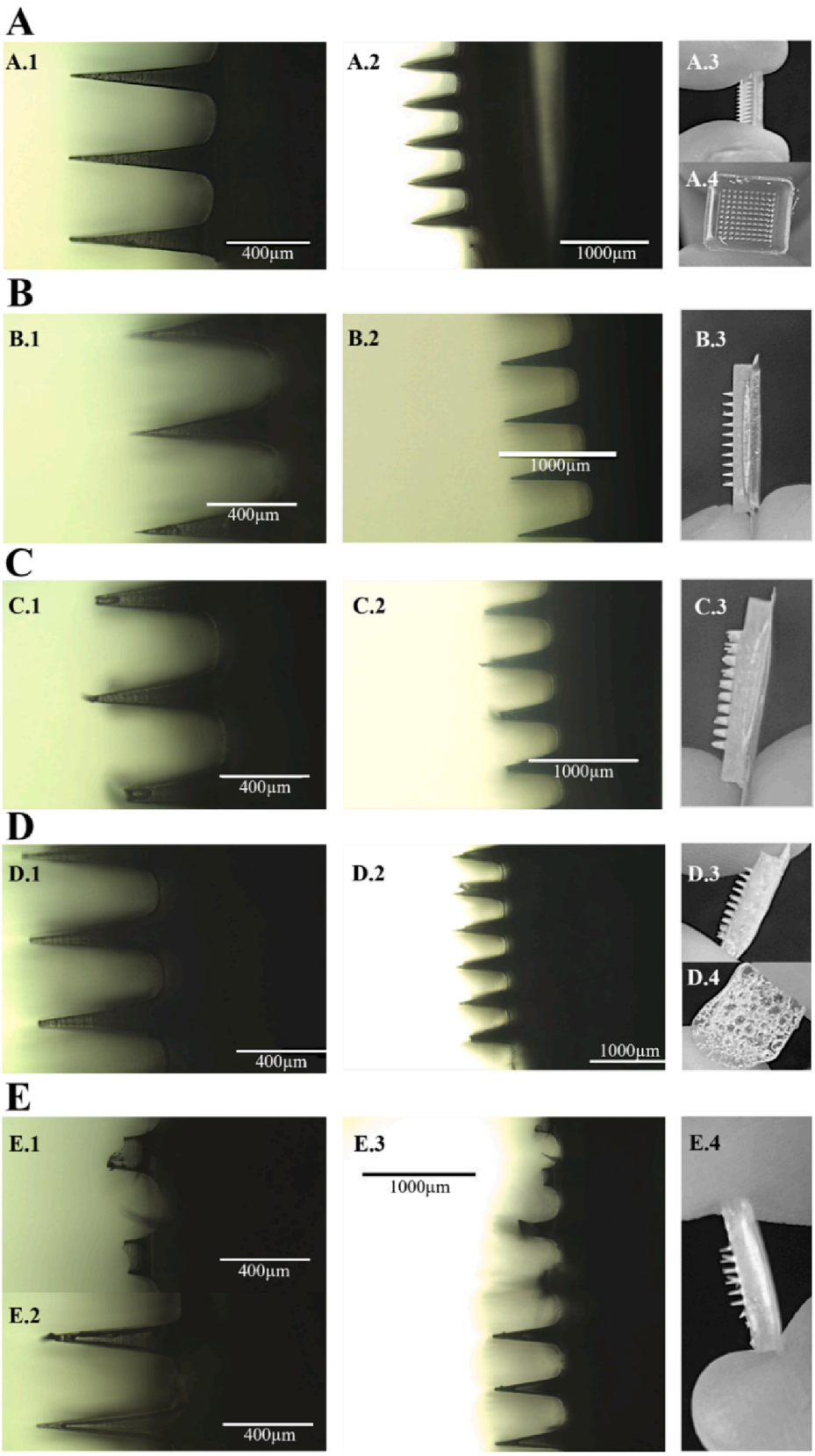

Fig. 3. Light microscopy images of the MN patches made of PMVE-MA (20 % w/v). (A) MNg - MNs obtained according to the general procedure, with centrifugation speed of 2,000 rcf and drying in desiccator; (B) MN1 – centrifugation speed 1,000 rcf; (C) MN2 – centrifugation speed of 500 rcf; (D) MN3 – vacuum oven used for drying the MNs; and (E) MN4 – MNs produced separately from the base. * Magnification of A1, B1, C1, D1, E1, E2 (10 ×) and A2, B2, C2, D2, and E3 (4 ×).

2.2.4.2. Parafilm penetration. The insertion capacity of plain MNs, PMVE-MA 20 % and HA 20 %, were tested using an 8-layered Parafilm®, as an elastic barrier that mimic the human skin (Fig. 2**B**). The MNs were placed on the top of the Parafilm® and the insertion was induced by Texture Analyser (TA CT3, AMETEK Brookfield, USA) using the same conditions as for the load at break test: 20 N, 0.5 mm/s, and 30 s. Then, the layers and the MNs-arrays were observed by light microscopy (EVOS xl, ThermoFisher, USA).

2.2.5. Microneedle penetration into porcine skin ex vivo

2.2.5.1. Dissolution studies. Ex vivo studies were performed using PMVE-MA (20 % w/v) and HA (20 % w/v) MNs to evaluate the dissolution capacity of each patch in contact with skin fluids. The MNs were placed on the top of the porcine skin (3 × 3 cm). The MNs were inserted in skin by Texture Analyser (20 N, 0.5 mm/s, and 30 s), (Fig. 2**C**). The MNs were removed from the skin after 20 and 60 s post-insertion and were examined by light microscopy.

3. Results and discussion

3.1. Dissolving MNs fabrication

Two different water-soluble polymers, PMVE-MA and HA were selected to fabricate the MN-arrays. In order to optimize the micromolding protocol for DMNs fabrication, PMVE-MA was chosen to produce the MNs due to its easy handling and low cost. The DMNs fabricated with 20 % (w/v) PMVE-MA showed remarkably uniformity (Fig. 3**A.1** and **3A.2**), namely a translucent base, confirming the reproducibility and ease of fabrication of this method.

A range of different centrifugation speeds was tested to accomplish a complete filling of the molds. A proper filling of the MNs molds was obtained with centrifugation speed down to 1000 rcf (Table 1; MN1), as shown in Fig. 3**B**. However, when decreasing the centrifugation speed to 500 rcf (Table 1; MN2), the filling of the molds was incomplete, and imperfections were observed in the MN array (Fig. 3**C**). The force provided with 500 rcf is not enough to deposit the viscous polymer solution into the mold holes. Furthermore, two drying setups at room temperature were tested: air-drying in desiccator and in vacuum oven. Drying of the MNs under vacuum (Table 1; MN3) resulted in an uniform shape of the MNs, as observed after demolding (Fig. 3**D.1** and **3D.2**). However, the base was not uniform and presenting a large number of bubbles (Fig. 3**D.4**) since the vacuum created a fast drying when compared to the conventional air drying (Table 1; MNg, MN1 and MN2). In MN4, producing the base separately from the MNs resulted in fragile broken MN-patches, as can be observed in Fig. 3**E.1** and **3E.3**. This may have occurred because of the reduced amount of polymer used to glue the MNs to the base layer. As it is observable in in MN4 (Fig. 3**E.2**) cavities are formed inside the MNs due to the air entrapment when gluing the base and the MNs together. According to Wang *et al.* forming cavities inside the MNs can be advantageous by improving drug delivery and providing faster release of a higher amount of drug, than compared with the traditional MNs. On the other hand, the cavities formation and bubbles accumulation inside the microneedles can negatively influence its mechanical properties, leading to a lower mechanical strength, therefore decreasing its penetration capability (Wang et al., 2016).

3.2. CM-coated MNs

Coating the MNs with CM was designed to provide a fast release after insertion into the skin. Furthermore, the accumulation of CM in the tips is crucial to ensure that it will reach the dendritic cells in the epidermis and dermis upon insertion into skin. HA with lower molecular weight can promote the immune system response, however, a very low molecular weight will negatively influence the mechanical strength of the MNs (Leone et al., 2020). Thus, a medium molecular weight of HA was chosen to provide a compromise between having enough mechanical strength of the MNs and adjuvant immune stimulation effect (Chi et al., 2022; Leone et al., 2019).

Coating of MNs started with the deposition of the CM in the mold, followed by polymer deposition. Different formulations (Table 2) were tested to achieve uniform distribution of CM in the coat to achieve an uniform tissue diffusion of CM after the insertion of MNs into the skin. When the CM was dispersed in water (Table 2; MN5) its distribution was not uniform, showing the presence of clusters (Fig. 4**A**). Two different sugars, sucrose and trehalose, were added to the CM solution (Table 2; MN6) to improve the stabilization of CM, by acting as protein stabilizers (Mistilis et al., 2017) during the drying process. Furthermore, P188 was added (Table 2; MNg1) to decrease the surface tension of the CM dispersion improving its distribution in the mold making the coat more uniform. The addition of the sugars (combination of sucrose and trehalose (5 % or 10 %)) enabled a better distribution of the CM coating on the MNs (Fig. 4**B**). Moreover, the distribution can be improved with the addition of P188 (0.5 or 1 %) resulting in a continuous and uniform layer of CM alongside the MN surface, due to its capability of reducing the surface tension and lowering the contact angle, as reported elsewhere (Gill and Prausnitz, 2007).

Once the MNs formulation with PMVE-MA (Table 2; MNg1, MN5, MN6) was optimized, new MNs were made using HA (Table 2; MN7). However, the HA MNs required further optimization because the CM was not uniformly distributed (Fig. 5**A**) as in the case of PMVE-MA (Fig. 4**C**). This can be attributed to different physical characteristics of

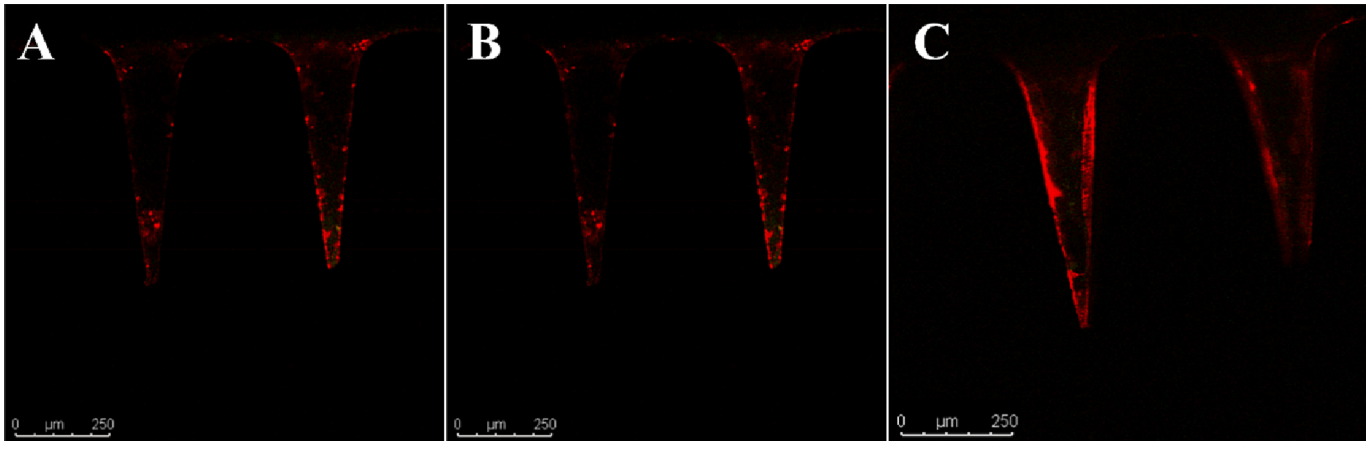

Fig. 4. Confocal microscopy images of CM-coated PMVE-MA (20 %) MNs (side view). CM (stained with CellMask™ Orange, in red) dispersed in water (A, MN5); in sucrose (5 %) and trehalose (5 %) (B, MN6); and in trehalose (5 %), sucrose (5 %) and P188 (0.5 %) (C, MNg1).

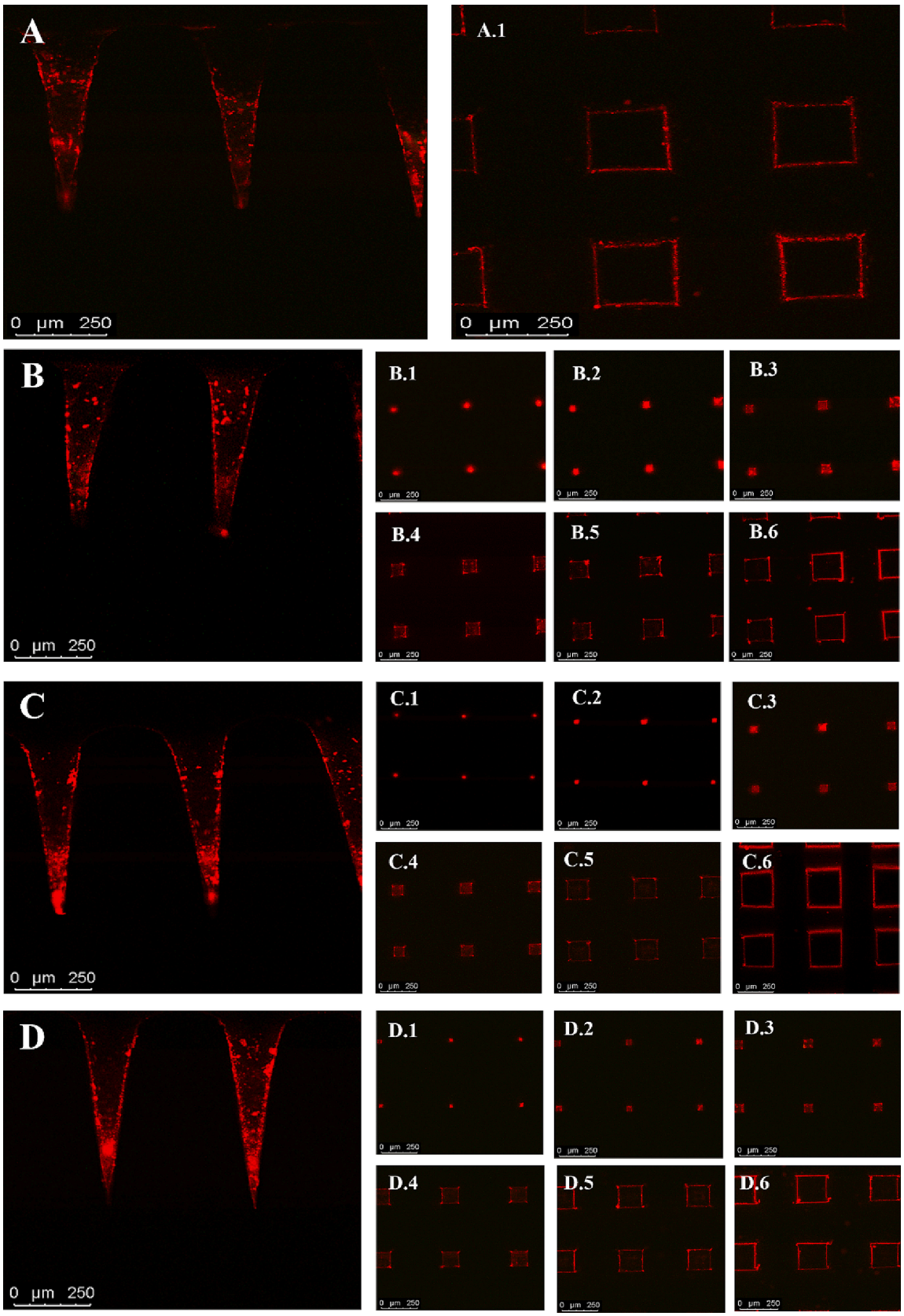

Fig. 5. Confocal microscopy of side and top views of CM-coated MNs. CM (stained with CellMask^{TM} Orange, in red) dispersed in trehalose (5 %), sucrose (5 %) and P188 (0.5 %) (A, MN7); in trehalose (5 %), sucrose (5 %), and Poloxamer 188 (0.5 %) with a pre-treatment with O_2 plasma was applied to the molds (B, MN8); in sucrose (10 %), trehalose (10 %) and Poloxamer 188 (1 %) (C, MN9); and in sucrose (10 %), trehalose (10 %), and Poloxamer 188 (1 %), with the CM concentration triplicated (D, MN10).*Selected polymer was HA (20 kDa) 20 % (w/v). ** Images in the sequence from 1 to 6 represent the top view of the MNs from the tip to the base.

HA, namely a higher viscoelasticity than PMVE-MA requiring the formulation to be adjusted. A pre-treatment of the negative molds with O_2 plasma (Table 2; MN8) was performed to increase their hydrophilicity and increase the interfacial area with the hydrophilic polymer (Nair et al., 2015) resulting in a higher accumulation of CM on the tips of the MNs (Fig. 5**B.1** and **5B.2**) in comparison with the non-treated molds (Fig. 5**A**). The same result was achieved when the concentration of sucrose, trehalose and P188 was doubled (MN9, Fig. 5**C.1** and **5C.2**). When the CM concentration was triplicated (Table 2; MN10), an efficient CM load was also accomplished (Fig. 5**D**).

3.3. CM-encapsulated MNs

In the encapsulation technique, the CM was mixed with the polymer solution and deposited in an one-step into the molds. Even though the encapsulation was different from the two-step coating; the results were comparable. Due to the drying pulling effect, the encapsulation resulted into the CM accumulation around the MNs, instead of being dispersed inside the polymer matrix (Fig. 6**A**). As indicated in Table 3, modifying the concentrations of sucrose, trehalose, P188 and PMVE-MA (doubled in MN12) led to the preparation of very fragile MNs. Preparing the MNs using HA (Table 3; MN13) instead of PMVE-MA resulted in similar accumulation of CM in the outside part of MNs (Fig. 6**B**). As a general result, the CM-encapsulated polymer formed a layer surrounding the MNs, even when the procedure was adjusted to provide multiple layers on the loaded polymer (Fig. 6**C**).

3.4. Mechanical properties

In order to produce MNs capable of piercing the skin, without breaking, and efficiently deliver drugs and biocargos, optimized mechanical strength and rigidity are required. The mechanical properties were evaluated by testing the MNs to fracture and insertion of MNs when submitted to a force mimicking the human thumb (20 N) (Larrañeta et al., 2014).

3.4.1. Fracture test (force at breakage)

To compare the two polymers, plain MNs of PMVE-MA and HA, both 20 % (w/v), were produced to perform the study. All MNs were observed under the microscope before and after compression (Fig. 7**A.1** and **7A.2**) against a solid surface (20 N for 30 s) using the Texture Analyser. Both MNs showed different behaviours. HA MNs showed tip bending without breaking (Fig. 7**A.3**). In contrast, PMVE-MA MNs showed tip and base breaking (Fig. 7**A.4**). These results indicate that HA has higher plasticity than PMVE-MA MNs which were more brittle, confirming the higher HA viscoelasticity, reported previously (Huang and Huang, 2018).

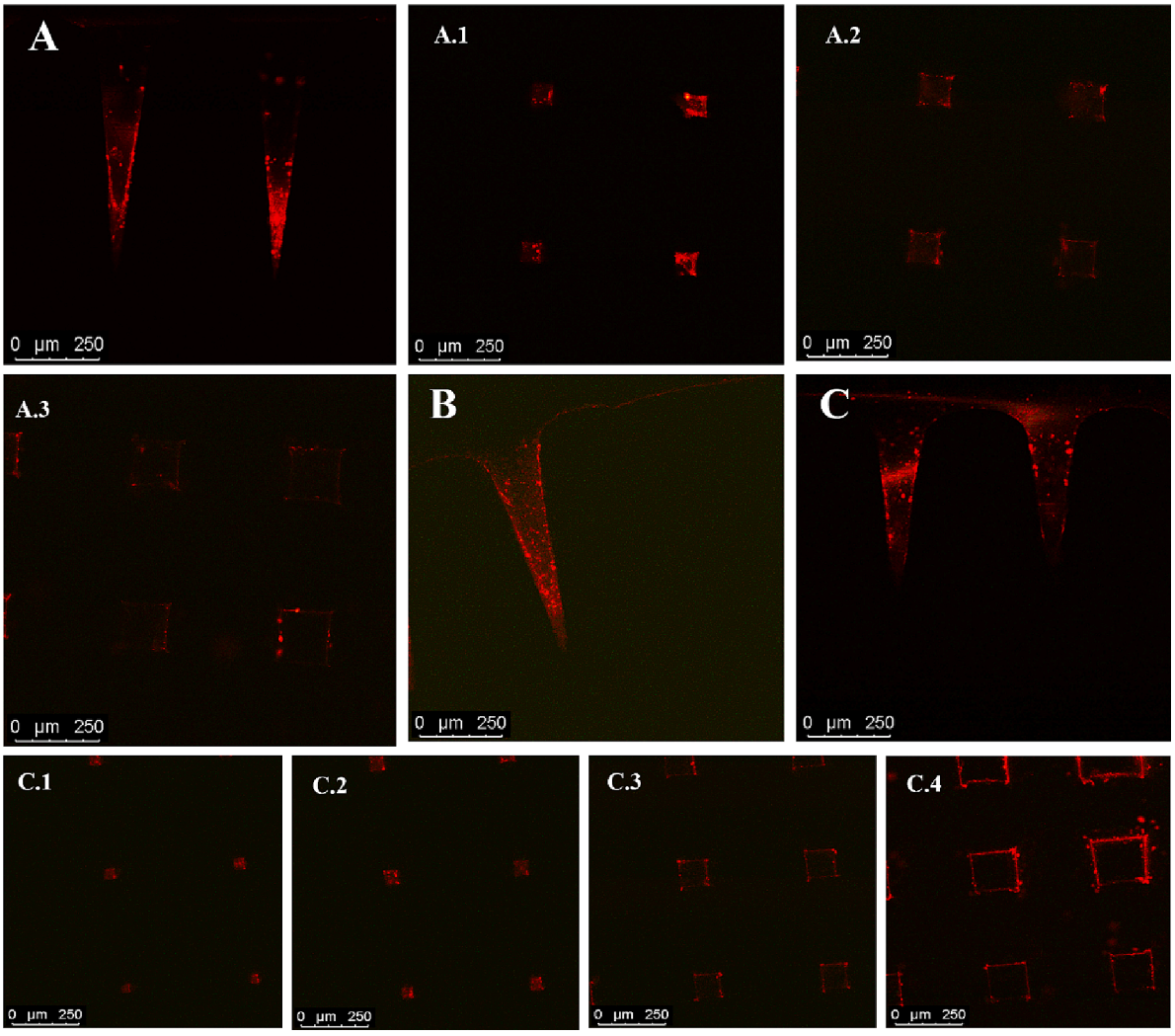

Fig. 6. Confocal microscopy of side and top view of CM-coated MNs. CM (stained with CellMask^{TM} Orange, in red) dispersed in trehalose (2.5 %), sucrose (2.5 %), P188 (0.25 %) and PMVE-MA (15 %) (A, MNg2); in trehalose (5 %), sucrose (5 %), and Poloxamer 188 (0.5 %) and PMVE-MA (30 %) (B, MN13); multilayering procedure where the CM is dispersed in trehalose (5 %), sucrose (5 %), P188 (0.5 %) and HA (20 %) (C, MN14).* The selected polymers were PMVE-MA (20 % w/v) (A) and HA (20 kDa) (20 % w/v) (B and C). ** Images in the sequence from 1 to 6 represent the top view of the MNs from the tip to the base.

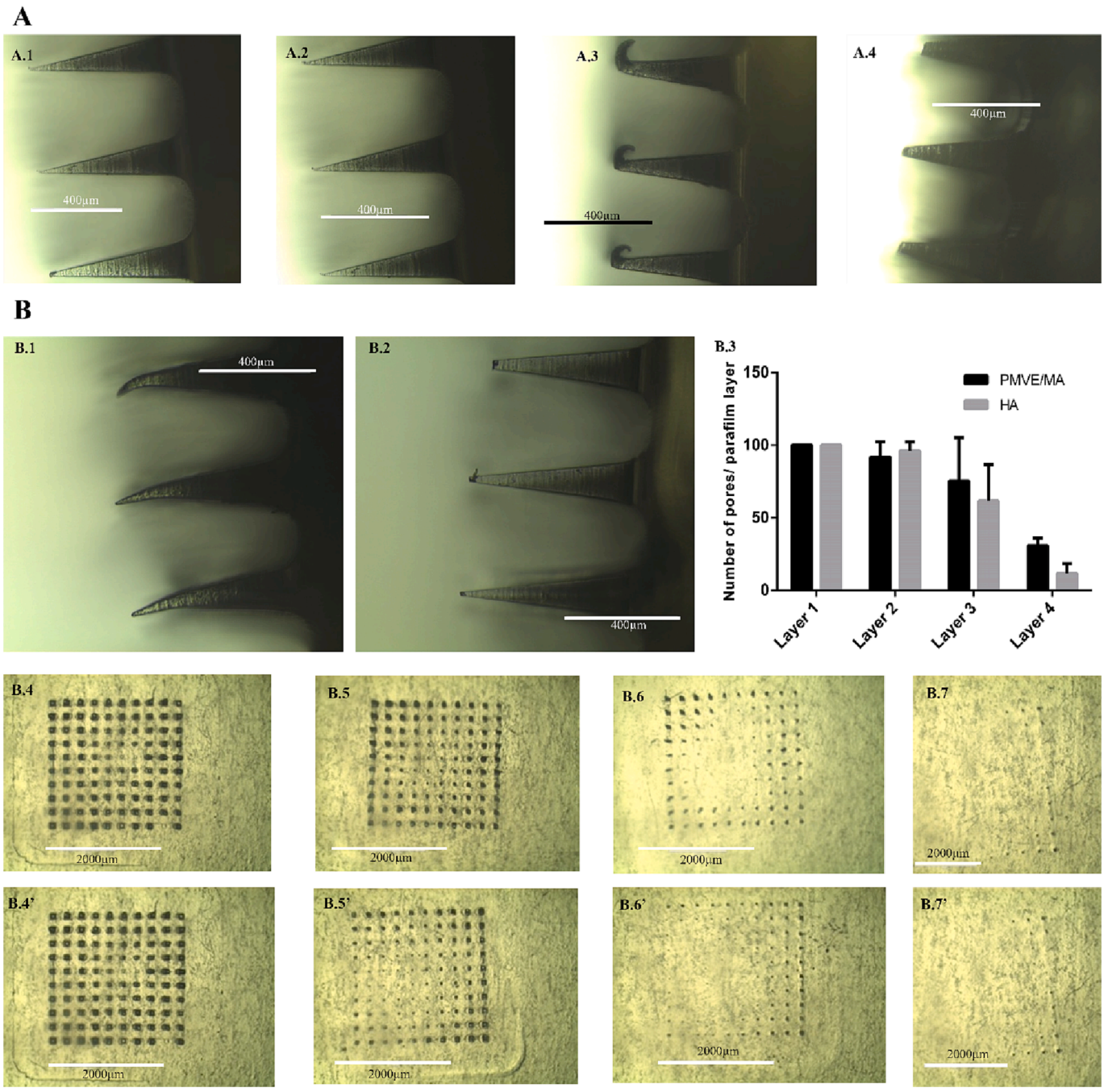

Fig. 7. (A) Light microscopy images of the MN patches before and after the compression test against 8 layers of Parafilm® using Texture Analyser (20 N for 30 s). (A.1-A.2): HA and PMVE-MA MNs, before compression, respectively. (A.3 and A.4): HA and PMVE-MA MNs after insertion, respectively. (B) Light microscopy images of the MNs patches after Parafilm® insertions. (B.1-B.2): HA MNs and PMVE-MA MNs, respectively, after insertion in 8 layers of parafilm using Texture Analyzer (20 N for 30 s). Parafilm layers after insertion with HA-MNs: (B.4) Layer number 1, (B.5) Layer number 2, (B.6) Layer number 3, (B.7) Layer number 4. Parafilm® layers after PMVE-MA MNs insertions: (B.4′) Layer number 1, (B.5′) Layer number 2, (B.6′) Layer number 3, (B.7′) Layer number 4.

Consequently, HA is preferred for the preparation of DMNs, compared to PMVE-MA without any additives. However, the mechanical properties of the PMVE-MA MNs can be improved if a plasticizer is used (Jin et al., 2022).

3.4.2. *Insertion evaluation*

To evaluate the insertion capability of PMVE-MA MNs and HA MNs, they were pressed against an elastic membrane consisting of 8 layers of folded Parafilm® using the Texture Analyzer (20 N, 30 s). Afterwards, the MNs were visualized by light microscopy, once removed from the parafilm. As expected, HA-MMs exhibited slightly bent tips (Fig. 7**B.1**), while PMVE-MA-MNs showed broken tips (Fig. 7**B.2**). Every Parafilm® layer (in the order of penetration, downwards) was observed under the microscope (Fig. 7**B.4-B.7** and **7B.4′-B.7′**) and the holes were counted (Fig. 7**B.3**), to test the penetration efficacy. Each layer of Parafilm® represented 127 µm. All MNs patches reached the fourth layer with an estimated penetration depth of 508 µm, which is hypothetically enough to reach deep in the epidermis layer, after human skin penetration. This is essential to efficiently deliver the CM and stimulate the APCs in the epidermis and generate the immune response (Glenn and Kenney, 2006; Michalak et al., 2021).

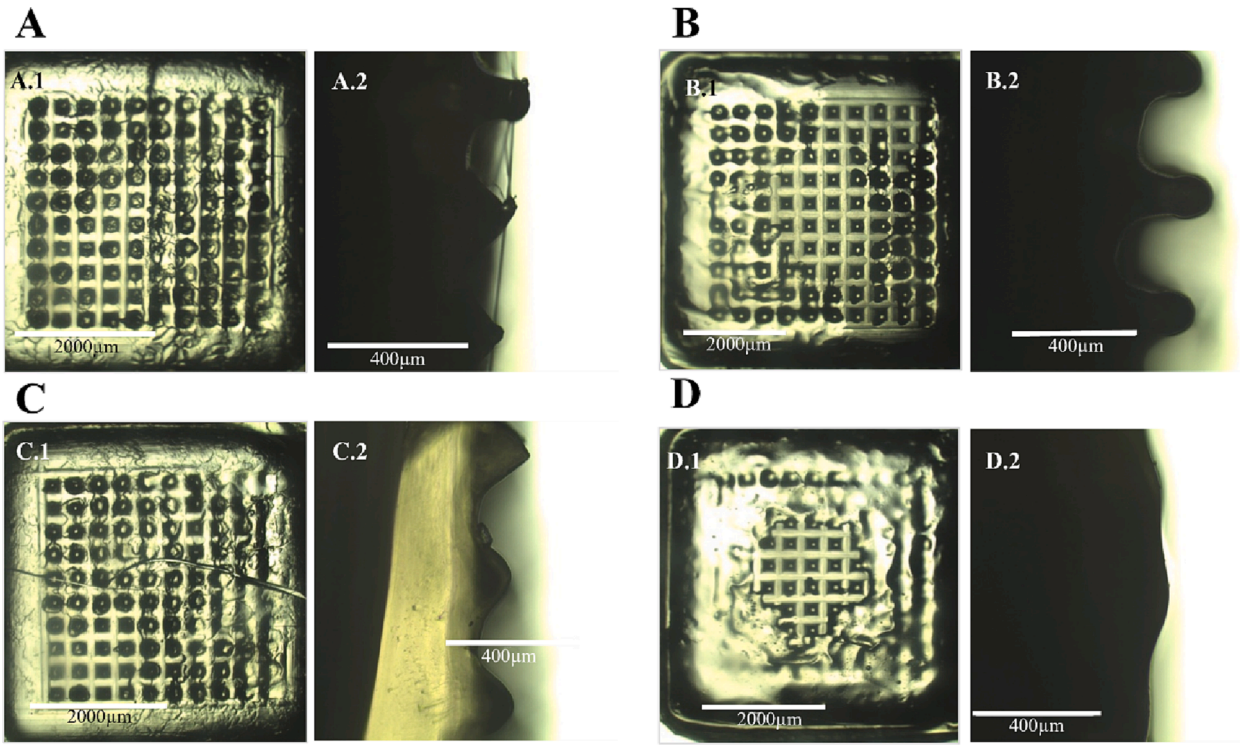

Fig. 8. Light microscopy images of PMVE-MA-MNs and HA-MNs after insertion in porcine skin using the Texture Analyser (30 N for 30 s). (A) The PMVE-MA MNs stayed in the skin for more 20 s, (B) the HA MNs stayed in the skin for more 20 s, (C) The PMVE-MA MNs stayed in the skin for more 60 s and (D) HA MNs stayed in the skin for more 60 s. (A1, B1, C1, and D1) top views of the patches. (A2, B2, C2, and D2) side views of the MNs.

3.5. Ex vivo MNs penetration into porcine skin

3.5.1. Dissolution studies

The dissolution of each plain PMVE-MA MNs and HA MNs were tested by insertion into the pork skin. Texture Analyser was used to compress the MNs against the skin surface (20 N for 30 s). After releasing the force, the MNs were left inside the skin for more 20 s and in another setup for 60 s. Afterwards, the MNs were visualized light microscopy (Fig. 8). Both types of MNs revealed a fast dissolution due to their water-soluble characteristics (Garland et al., 2014). Approximately 30 s was sufficient for the dissolution of both polymers, PMVE-MA (Fig. 8**A**) and HA (Fig. 8**B**), indicating the suitability of both polymers for the development of fast dissolving MNs. After 60 s of insertion almost completed dissolution was achieved, although, when compared to PMVE-MA MNs (Fig. 8C), HA-MNs have shown a faster dissolution (Fig. 8**D**).

4. Conclusions

An optimized and detailed protocol, to produce fast dissolving MNs, was successfully developed and achieved. Fast dissolving MNs were developed for the delivery of B16F10 melanoma CM. The MNs were successfully prepared using PMVE-MA and HA. The MNs fabrication by the micromolding technique was optimized for the processing factors (centrifugation force and drying method). Preparation of CM-coated MNs and concentration of the CM in the tip of the MNs was a preferable approach for fast delivery of the CM to APCs in skin. The coating of CM was optimized to achieve an uniformly distributed coat around the MNs. Sucrose and trehalose were added to CM solution to enhance the CM proteins stability during MNs preparation and drying. P188 was also added to decrease the surface tension of the CM and increase its accumulation inside the mold for efficient loading. Both PMVE-MA and HA are efficient candidates for the development of fast dissolving MNs, as proved by their fast dissolution (in about 30 s) after insertion of the MNs in porcine skin *ex vivo*. However, HA stays more preferable to PMVE-MA due to its superior mechanical properties and resistance to fracture upon compression. Overall, the elaborated protocol provides support and more extensive information on the procedure itself to fulfil the lack of guidance on how to overcome the initial challenges related to the development of dissolving MNs loaded with biological materials. The B16F10 melanoma CM-dissolving MNs were efficiently developed with a promising structure for further use for immunotherapy and melanoma applications.

CRediT authorship contribution statement

Maria C. Lobita: Conceptualization, Methodology, Visualization, Investigation, Writing – original draft. **Nesma El-Sayed:** Conceptualization, Methodology, Visualization, Investigation, Supervision. **João F. Pinto:** Supervision. **Hélder A. Santos:** Conceptualization, Methodology, Supervision.

Declaration of Competing Interest

The authors declare that they have no known competing financial interests or personal relationships that could have appeared to influence the work reported in this paper.

Data availability

Data will be made available on request.

Acknowledgements

Prof. Santos acknowledges the financial support from Business Finland (Project no. 1179/31/2020), the Academy of Finland (No. 331151) and the UMCG Research Funds for financial support.

References

Aich, K., Singh, T., Dang, S., 2022. Advances in microneedle-based transdermal delivery for drugs and peptides. Drug Deliv. Transl. Res. 12, 1556–1568. https://doi.org/10.1007/s13346-021-01056-8.

Ali, M., Namjoshi, S., Benson, H.A., Mohammed, Y., Kumeria, T., 2022. Dissolvable polymer microneedles for drug delivery and diagnostics. J. Control. Release 347, 561–589. https://doi.org/10.1016/j.jconrel.2022.04.043.

Amani, H., Shahbazi, M.A., D'Amico, C., Fontana, F., Abbaszadeh, S., Santos, H.A., 2021. Microneedles for painless transdermal immunotherapeutic applications. J. Control. Release 330, 185–217. https://doi.org/10.1016/j.jconrel.2020.12.019.

Baeva, L.F., Lyle, D.B., Rios, M., Langone, J.J., Lightfoote, M.M., 2014. Different molecular weight hyaluronic acid effects on human macrophage interleukin 1β production. J. Biomed. Mater. Res. - Part A 102, 305–314. https://doi.org/10.1002/jbm.a.34704.

Bauleth-Ramos, T., El-Sayed, N., Fontana, F., Lobita, M., Shahbazi, M.-A., Santos, H., 2023. Recent Approaches for Enhancing the Performance of Dissolving Microneedles in Drug Delivery Applications. Mater. Today.

Cheng, Y., Bo, H., Qin, R., Chen, F., Xue, F., An, L., Huang, G., 2022. Hyaluronic acid - coated Bi : Cu 2 O : an - H 2 S - responsive agent for colon cancer with targeted delivery and enhanced photothermal performance 1–14. https://doi.org/10.1186/s12951-022-01555-x.

Chi, Y., Huang, Y., Kang, Y., Dai, G., Liu, Z., Xu, K., Zhong, W., 2022. The effects of molecular weight of hyaluronic acid on transdermal delivery efficiencies of dissolving microneedles. Eur. J. Pharm. Sci. 168, 106075 https://doi.org/10.1016/j.ejps.2021.106075.

Dalvi, M., Kharat, P., Thakor, P., Bhavana, V., Singh, S.B., Mehra, N.K., 2021. Panorama of dissolving microneedles for transdermal drug delivery. Life Sci. 284, 119877 https://doi.org/10.1016/j.lfs.2021.119877.

D'Amico, C., Fontana, F., El-Sayed, N., Elbadri, K., Correia, A., Rahikkala, A., Saarinen, J., Shahbazi, M.A., Santos, H.A., 2023. Double-Layered Polyvinylpyrrolidone–Poly(methyl vinyl ether-alt-maleic acid)-Based Microneedles to Deliver Meloxicam: An In Vitro, In Vivo, and Short-Term Stability Evaluation Study. Adv. Ther. 2300138, 1–10. https://doi.org/10.1002/adtp.202300138.

Davis, L.E., Shalin, S.C., Tackett, A.J., 2019. Current state of melanoma diagnosis and treatment. Cancer Biol. Ther. 20, 1366–1379. https://doi.org/10.1080/15384047.2019.1640032.

Demir, Y.K., Metin, A.Ü., Şatıroğlu, B., Solmaz, M.E., Kayser, V., Mäder, K., 2017. Poly (methyl vinyl ether-co-maleic acid) – Pectin based hydrogel-forming systems: Gel, film, and microneedles. Eur. J. Pharm. Biopharm. 117, 182–194. https://doi.org/10.1016/j.ejpb.2017.04.018.

El-Sayed, N., Vaut, L., Schneider, M., 2020. Customized fast-separable microneedles prepared with the aid of 3D printing for nanoparticle delivery. Eur. J. Pharm. Biopharm. 154, 166–174. https://doi.org/10.1016/j.ejpb.2020.07.005.

Fusciello, M., Fontana, F., Tähtinen, S., Capasso, C., Feola, S., Martins, B., Chiaro, J., Peltonen, K., Ylösmäki, L., Ylösmäki, E., Hamdan, F., Kari, O.K., Ndika, J., Alenius, H., Urtti, A., Hirvonen, J.T., Santos, H.A., Cerullo, V., 2019. Artificially cloaked viral nanovaccine for cancer immunotherapy. Nat. Commun. 10, 1–13. https://doi.org/10.1038/s41467-019-13744-8.

Garland, M.J., Salvador, E.C., Migalska, K., Woolfson, A.D., Donnelly, R.F., 2014. Europe PMC Funders Group Dissolving polymeric microneedle arrays for electrically assisted transdermal drug delivery. J. Control. Release 159, 52–59. https://doi.org/10.1016/j.jconrel.2012.01.003.Dissolving.

Gera, A.K., Burra, R.K., 2022. The Rise of Polymeric Microneedles: Recent Developments, Advances, Challenges, and Applications with Regard to Transdermal Drug Delivery. J. Funct. Biomater. 13, 81. https://doi.org/10.3390/jfb13020081.

Gill, H.S., Prausnitz, M.R., 2007. Coating formulations for microneedles. Pharm. Res. 24, 1369–1380. https://doi.org/10.1007/s11095-007-9286-4.

Glenn, G.M., Kenney, R.T., 2006. Mass vaccination: Solutions in the skin. Curr. Top. Microbiol. Immunol. 304, 247–268. https://doi.org/10.1007/3-540-36583-4_14.

Guillot, A.J., Cordeiro, A.S., Donnelly, R.F., Montesinos, M.C., Garrigues, T.M., Melero, A., 2020. Microneedle-based delivery: An overview of current applications and trends. Pharmaceutics 12, 1–28. https://doi.org/10.3390/pharmaceutics12060569.

Guillot, A.J., Martínez-Navarrete, M., Zinchuk-Mironova, V., Melero, A., 2023. Microneedle-assisted transdermal delivery of nanoparticles: Recent insights and prospects. Wiley Interdiscip. Rev. Nanomedicine Nanobiotechnology 1–30. https://doi.org/10.1002/wnan.1884.

Hong, X., Wei, L., Wu, F., Wu, Z., Chen, L., Liu, Z., Yuan, W., 2013. Dissolving and biodegradable microneedle technologies for transdermal sustained delivery of drug and vaccine. Drug Des. Devel. Ther. 7, 945–952. https://doi.org/10.2147/DDDT.S44401.

Huang, G., Huang, H., 2018. Application of hyaluronic acid as carriers in drug delivery. Drug Deliv. 25, 766–772. https://doi.org/10.1080/10717544.2018.1450910.

Huang, S., Liu, H., Huang, S., Fu, T., Xue, W., Guo, R., 2020. Dextran methacrylate hydrogel microneedles loaded with doxorubicin and trametinib for continuous transdermal administration of melanoma. Carbohydr. Polym. 246, 116650 https://doi.org/10.1016/j.carbpol.2020.116650.

Imlimthan, S., Khng, Y.C., Keinänen, O., Zhang, W., Airaksinen, A.J., Kostiainen, M.A., Zeglis, B.M., Santos, H.A., Sarparanta, M., 2021. A Theranostic Cellulose Nanocrystal-Based Drug Delivery System with Enhanced Retention in Pulmonary Metastasis of Melanoma. Small 17. https://doi.org/10.1002/smll.202007705.

Ita, K., 2017. Dissolving microneedles for transdermal drug delivery: Advances and challenges. Biomed. Pharmacother. 93, 1116–1127. https://doi.org/10.1016/j.biopha.2017.07.019.

Jin, M., Jeon, W.-J., Lee, H., Jung, M., Kim, H.-E., Yoo, H., Won, J.-H., Kim, J.C., Park, J.-H., Yang, M.-J., Lee, H.-K., Cho, C.-W., 2022. Preparation and evaluation of rapid disintegrating formulation from coated microneedle. Drug Deliv. Transl. Res. 12, 415–425. https://doi.org/10.1007/s13346-021-01046-w.

Kim, M.H., Nguyen, D.T., Kim, D.D., 2022. Recent studies on modulating hyaluronic acid-based hydrogels for controlled drug delivery. J. Pharm. Investig. 52, 397–413. https://doi.org/10.1007/s40005-022-00568-w.

Larrañeta, E., Moore, J., Vicente-Pérez, E.M., González-Vázquez, P., Lutton, R., Woolfson, A.D., Donnelly, R.F., 2014. A proposed model membrane and test method for microneedle insertion studies. Int. J. Pharm. 472, 65–73. https://doi.org/10.1016/j.ijpharm.2014.05.042.

Leone, M., Priester, M.I., Romeijn, S., Nejadnik, M.R., Mönkäre, J., O'Mahony, C., Jiskoot, W., Kersten, G., Bouwstra, J.A., 2019. Hyaluronan-based dissolving microneedles with high antigen content for intradermal vaccination: Formulation, physicochemical characterization and immunogenicity assessment. Eur. J. Pharm. Biopharm. 134, 49–59. https://doi.org/10.1016/j.ejpb.2018.11.013.

Leone, M., Romeijn, S., Slütter, B., O'Mahony, C., Kersten, G., Bouwstra, J.A., 2020. Hyaluronan molecular weight: Effects on dissolution time of dissolving microneedles in the skin and on immunogenicity of antigen. Eur. J. Pharm. Sci. 146, 105269 https://doi.org/10.1016/j.ejps.2020.105269.

Lesterhuis, W.J., Haanen, J.B.A.G., Punt, C.J.A., 2011. Cancer immunotherapy-revisited. Nat. Rev. Drug Discov. 10, 591–600. https://doi.org/10.1038/nrd3500.

Liu, C., Liu, Y., Yu, Y., Zhao, Y., Yu, A., 2022. Comprehensive analysis of ferroptosis-related genes and prognosis of cutaneous melanoma. BMC Med. Genomics 15, 1–17. https://doi.org/10.1186/s12920-022-01194-z.

Liu, T., Luo, G., Xing, M., 2020. Biomedical Applications of Polymeric Microneedles for Transdermal Therapeutic Delivery and Diagnosis: Current Status and Future Perspectives. Adv. Ther. 3, 1–15. https://doi.org/10.1002/adtp.201900140.

Matsuo, K., Yokota, Y., Zhai, Y., Quan, Y.S., Kamiyama, F., Mukai, Y., Okada, N., Nakagawa, S., 2012. A low-invasive and effective transcutaneous immunization system using a novel dissolving microneedle array for soluble and particulate antigens. J. Control. Release 161, 10–17. https://doi.org/10.1016/j.jconrel.2012.01.033.

Mbituyimana, B., Ma, G., Shi, Z., Yang, G., 2022. Polymeric microneedles for enhanced drug delivery in cancer therapy. Biomater. Adv. 142, 213151 https://doi.org/10.1016/j.bioadv.2022.213151.

Michalak, M., Pierzak, M., Kręcisz, B., Suliga, E., 2021. Bioactive compounds for skin health: A review. Nutrients 13, 1–31. https://doi.org/10.3390/nu13010203.

Mistilis, M.J., Joyce, J.C., Esser, E.S., Skountzou, I., Compans, R.W., Bommarius, A.S., Prausnitz, M.R., 2017. Long-term stability of influenza vaccine in a dissolving microneedle patch. Drug Deliv. Transl. Res. 7, 195–205. https://doi.org/10.1007/s13346-016-0282-2.

Naing, A., Hajjar, J., 2018. Advances in Experimental Medicine and Biology: Immunotherapy.

Nair, K., Whiteside, B., Grant, C., Patel, R., Tuinea-Bobe, C., Norris, K., Paradkar, A., 2015. Investigation of plasma treatment on micro-injection moulded microneedle for drug delivery. Pharmaceutics 7, 471–485. https://doi.org/10.3390/pharmaceutics7040471.

Park, J.H., Allen, M.G., Prausnitz, M.R., 2005. Biodegradable polymer microneedles: Fabrication, mechanics and transdermal drug delivery. J. Control. Release 104, 51–66. https://doi.org/10.1016/j.jconrel.2005.02.002.

Park, W., Seong, K.Y., Han, H.H., Yang, S.Y., Hahn, S.K., 2021. Dissolving microneedles delivering cancer cell membrane coated nanoparticles for cancer immunotherapy. RSC Adv. 11, 10393–10399. https://doi.org/10.1039/d1ra00747e.

Park, J.H., Yoon, Y.K., Choi, S.O., Prausnitz, M.R., Allen, M.G., 2007. Tapered conical polymer microneedles fabricated using an integrated lens technique for transdermal drug delivery. IEEE Trans. Biomed. Eng. 54, 903–913. https://doi.org/10.1109/TBME.2006.889173.

Prausnitz, M.R., 2004. Microneedles for transdermal drug delivery. Adv. Drug Deliv. Rev. 56, 581–587. https://doi.org/10.1016/j.addr.2003.10.023.

Rawlings, A.V., Harding, C.R., 2004. Moisturization and skin barrier function. Dermatol. Ther. 17, 43–48. https://doi.org/10.1111/j.1396-0296.2004.04s1005.x.

Sabbagh, F., Kim, B.S., 2022. Recent advances in polymeric transdermal drug delivery systems. J. Control. Release 341, 132–146. https://doi.org/10.1016/j.jconrel.2021.11.025.

Sabri, A.H., Kim, Y., Marlow, M., Scurr, D.J., Segal, J., Banga, A.K., Kagan, L., Lee, J.B., 2020. Intradermal and transdermal drug delivery using microneedles – Fabrication, performance evaluation and application to lymphatic delivery. Adv. Drug Deliv. Rev. 153, 195–215. https://doi.org/10.1016/j.addr.2019.10.004.

Sadeqi, A., Kiaee, G., Zeng, W., Rezaei Nejad, H., Sonkusale, S., 2022. Hard polymeric porous microneedles on stretchable substrate for transdermal drug delivery. Sci. Rep. 12, 1–10. https://doi.org/10.1038/s41598-022-05912-6.

Schmidt, J., Pilbauerova, N., Soukup, T., Suchankova-Kleplova, T., Suchanek, J., 2021. Low molecular weight hyaluronic acid effect on dental pulp stem cells in vitro. Biomolecules 11, 1–16. https://doi.org/10.3390/biom11010022.

Singh, P., Carrier, A., Chen, Y., Lin, S., Wang, J., Cui, S., Zhang, X., 2019. Polymeric microneedles for controlled transdermal drug delivery. J. Control. Release 315, 97–113. https://doi.org/10.1016/j.jconrel.2019.10.022.

Tran, K.T.M., Gavitt, T.D., Farrell, N.J., Curry, E.J., Mara, A.B., Patel, A., Brown, L., Kilpatrick, S., Piotrowska, R., Mishra, N., Szczepanek, S.M., Nguyen, T.D., 2021. Transdermal microneedles for the programmable burst release of multiple vaccine payloads. Nat. Biomed. Eng. 5, 998–1007. https://doi.org/10.1038/s41551-020-00650-4.

Wang, Y., Tang, Z., Guo, X., Zhao, Y., Ren, S., Zhang, Z., Lv, H., 2022. Hyaluronic acid-cyclodextrin encapsulating paeonol for treatment of atopic dermatitis. Int. J. Pharm. 623, 121916 https://doi.org/10.1016/j.ijpharm.2022.121916.

Wang, Q.L., Zhu, D.D., Liu, X.B., Chen, B.Z., Guo, X.D., 2016. Microneedles with controlled bubble sizes and drug distributions for efficient transdermal drug delivery. Sci. Rep. 6, 1–11. https://doi.org/10.1038/srep38755.

Yenkoidiok-Douti, L., Barillas-Mury, C., Jewell, C.M., 2021. Design of dissolvable microneedles for delivery of a PFS47-based malaria transmission-blocking vaccine. ACS Biomater. Sci. Eng. 7, 1854–1862. https://doi.org/10.1021/acsbiomaterials.0c01363.

Zeng, Q., Gammon, J.M., Tostanoski, L.H., Chiu, Y.C., Jewell, C.M., 2017. In Vivo Expansion of Melanoma-Specific T Cells Using Microneedle Arrays Coated with Immune-Polyelectrolyte Multilayers. ACS Biomater. Sci. Eng. 3, 195–205. https://doi.org/10.1021/acsbiomaterials.6b00414.

Zhang, X., Wang, Y., Chi, J., Zhao, Y., 2020. Smart Microneedles for Therapy and Diagnosis. Research 2020, 1–26. https://doi.org/10.34133/2020/7462915.

Zhu, H., Mah Jian Qiang, J., Wang, C.G., Chan, C.Y., Zhu, Q., Ye, E., Li, Z., Loh, X.J., 2022. Flexible polymeric patch based nanotherapeutics against non-cancer therapy. Bioact. Mater. 18, 471–491. https://doi.org/10.1016/j.bioactmat.2022.03.034.